$$C_{fN}=2g''_W K_{11}C^2C_R/R_{e\theta}/\epsilon, \quad S_{NN}=L_{22}K_{11}C^2C_R/R_{e\theta}/\epsilon$$

$$\theta_{12}=\theta_{11}C(K_{12}/K_{11}-\epsilon b/K_{11}), \quad \theta_{121}=\theta_{11}CK_{12}/K_{11}-\delta_{21}$$

$$\theta_{112}=\theta_{11}C(K_{112}/K_{11}-\epsilon b/K_{11})$$

$$\theta_{221}=\theta_{11}C^2K_{221}/K_{11}, \quad S_{TN}=L_{12}K_{11}CC_R/R_{e\theta}$$

## References


[1] Prandtl, L., "On Boundary Layers in Three-Dimensional Flow," *Ministry Aircraft Production* (Volkenrode), *Reports and Translations*, Vol. 64, May 1946.

[2] Struminskii, V. V., "Sideslip in a Viscous Compressible Gas," NACA TM 1276, 1951.

[3] Jones, R. T., "Effects of Sweepback on Boundary Layer and Separation," NACA TN 1402, 1947.

[4] Sears, W. R., "The Boundary Layer of Yawed Cylinders," *Journal of Aeronautical Sciences*, Vol. 15, Jan. 1948, pp. 49-52.

[5] Cooke, J. C., "The Boundary Layer of a Class of Infinite Yawed Cylinders," *Proceedings of Cambridge Philosophical Society*, Vol. 46, 1950, pp. 645-648.

[6] Cumpsty, N. A. and Head, M. R., "The Calculation of the Three-Dimensional Turbulent Boundary Layers, Part I," *Aeronautical Quarterly*, Vol. 18, Feb. 1967, pp. 55-83.

[7] Mager, A., "Generalization of Boundary Layer Momentum Integral Equations to Three Dimensional Flows Including Those of Rotating Systems," NACA Rept. 1067, 1952.

[8] Thompson, B. G. J., "A New Two-Parameter Family of Mean Velocity Profiles for Incompressible Turbulent Boundary Layers on Smooth Walls," ARC R&M 3463, 1965.

[9] Stock, H. W., "Integral Method for the Calculation of Three-Dimensional Laminar and Turbulent Boundary Layers," NASA TM-75320, 1978.

[10] Squire, L. C., "The Three Dimensional Boundary-Layer Equations and Some Power Series Solutions," ARC R&M 3005, 1957.

[11] Myring, D. F., "An Integral Prediction Method for Three-Dimensional Turbulent Boundary Layers in Incompressible Flow," RAE TR 70147, 1970.

[12] Smith, P. D., "An Integral Prediction Method for Three-Dimensional Compressible Turbulent Boundary Layers," ARC R&M 3739, 1974.


AIAA 82-4096

# Similarity Relation for Vortex-Asymmetry Onset on Slender Pointed Forebodies


Henry W. Woolard*

*Air Force Wright Aeronautical Laboratories, Wright Patterson Air Force Base, Ohio*


## Introduction

THE subject of similarity conditions for the onset of vortex asymmetry for laterally symmetric flow (zero sideslip) over slender pointed forebodies and wings at high angles of attack at subsonic speeds has been explored from an experimental viewpoint by Keener and Chapman.[1] The subject has been further addressed by Ericsson and Reding in their comprehensive survey paper[2] on vortex-induced asymmetric loads. Ericsson and Reding emphasize the importance of forebody asymmetric vortices and observe that, for slender pointed bodies with an afterbody, the available evidence indicates that the nose-generated vortices not only are responsible for the larger asymmetric loads but also influence greatly the vortex shedding over the afterbody.

Although a number of aerodynamic schemes for attenuating or eliminating vortex-induced asymmetric loads on forebodies are known, the actual cause of the vortex-asymmetry onset phenomenon is not completely understood. There are at least two schools of thought on a possible cause for the asymmetry onset. One school proposes that a peripheral asymmetry of the viscous flow separation points precipitates the vortex asymmetry, whereas another school believes that an inviscid hydrodynamic instability due to the crowding together of the symmetric vortex pair is responsible for the asymmetry.

On the basis of some comparisons with a limited amount of experimental data, Keener and Chapman[1] show that, at high angles of attack and zero sideslip, an asymmetric moment (in roll) occurs on slender delta wings which is similar to the occurrence of an asymmetric force (side force) on slender circular forebodies. They comment that since the asymmetry in the forebody forces is known to be associated with an asymmetry in the vortex flowfield on the lee side, the asymmetry in the wing rolling moment must be associated with a similar asymmetry in the wing vortex flowfield. The fact that the angle of attack at which asymmetry occurs decreases with increasing slenderness suggested to Keener and Chapman that the cause of the vortex asymmetry is a hydrodynamic instability in the vortex flowfield resulting from the crowding together of the vortices as the apex angle is decreased. It is further suggested by the aforementioned investigators that the fact that the separation point is fixed at the leading edge for delta wings implies that an asymmetry in the separation points on a body of revolution is not necessarily an essential feature of vortex asymmetry.

It is the purpose of this Note to provide an approximate theoretical basis for the experimental observations of Keener and Chapman.[1]

## Analysis

The analysis employs slender-body theory, with the various cross-flow planes used summarized in Fig. 1. Except for the $\hat{X}$ and $\bar{X}$ planes, all paired planes (denoted by the arrows on the figure) are conformally mapped onto each other. A cross section of the flow about the subject forebody at a given $x$ station (viewed looking upstream) is shown in Fig. 1a. Body axes $x$, $y$, and $z$ are employed, with the $x$ axis positive in the general direction of the positive freestream $U_\infty$. The cross-flow velocity components $v$ and $w$ are respectively parallel to $y$ and $z$. The complex variable for the $X$ plane is $X=y+iz$. For a complex potential defined by $W=\phi+i\Psi$, the conjugate complex velocity is given by $v-iw=\mathrm{d}W/\mathrm{d}X$. The angle of attack $\alpha$ is given by $\alpha=w_\infty/U_\infty$. Corresponding quantities in cross-flow planes other than the $X$ plane are denoted by applying the overscript or superscript symbol (tilde, caret, bar, or asterisk) appropriate to the particular plane under consideration, as shown in Fig. 1. The body cross section shown in Fig. 1a is an ellipse, although any cross-sectional shape that can be mapped conformally into a circle may be analyzed. The freestream velocity $U_\infty$, the lateral dimension $a(x)$, and the $x$ coordinate are invariant from cross-flow plane to cross-flow plane. The latter condition requires identical planforms (not restricted to straight leading edges) for the variously transformed bodies.

The purpose of the cross-flow plane progressions shown in Fig. 1 is to relate the flow about an arbitrary laterally symmetric thick body having arbitrarily located laterally symmetric separation points $s$ and $s'$ in the $X$ plane to the flow about a zero-thickness wing of a similar planform shape with separation points $s$ and $s'$ at the wing leading edges in the $X^*$ plane. In contrast to the usual mapping procedure wherein the

Received May 15, 1981; revision received Sept. 14, 1981. 

*Aerospace Engineer, Flight Dynamics Laboratory, Flight Control Division, Control Dynamics Branch (AFWAL/FIGC). Associate Fellow AIAA.

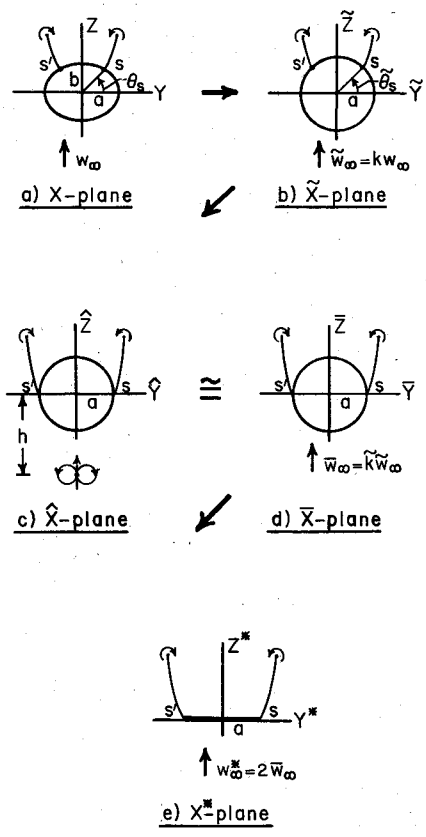


**Fig. 1 Illustration of cross-flow planes.**

cross-flow velocity at infinity is preserved, the present procedure preserves the body lateral dimensions $a(x)$, with a consequent nonunity scaling of the cross-flow velocity at infinity.

For those plane-to-plane progressions for which conformal transformations are involved, the appropriate transformation relations are

$$X=(a+b)(\tilde{X}/2a)+a(a-b)/2\tilde{X} \tag{1}$$

$$(\tilde{X}-ia)/(\tilde{X}+ia)=(\hat{X}-ia)(1-\sin\tilde{\theta}_s)/(\hat{X}+ia)\cos\tilde{\theta}_s \tag{2}$$

$$X^*=(1/2)[\bar{X}+(a^2/\bar{X})] \tag{3}$$

The cross-flow stream velocity scaling factor $k$ (see Fig. 1) and the relation between the separation points in the $X$ and $\tilde{X}$ planes are given, respectively, by

$$k=(a+b)/2a \tag{4}$$

$$\tan\tilde{\theta}_s=(a/b)\tan\theta_s \qquad (a\neq 0,\quad b\neq 0) \tag{5}$$

The uniform cross-flow stream at infinity in the $\tilde{X}$ plane transforms into a doublet at the point $\hat{X}=-ih$ in the $\hat{X}$ plane. The doublet location is related to the locations of the separation points in the $\hat{X}$ plane by

$$a/h=\tan(\tilde{\theta}_s/2) \tag{6}$$

The doublet complex potential is determined by transforming the complex potential $W=-i\tilde{w}_\infty\tilde{X}$ for a uniform vertical flow in the $\tilde{X}$ plane onto the $\hat{X}$ plane via the transformation of Eq. (2). The corresponding doublet conjugate complex

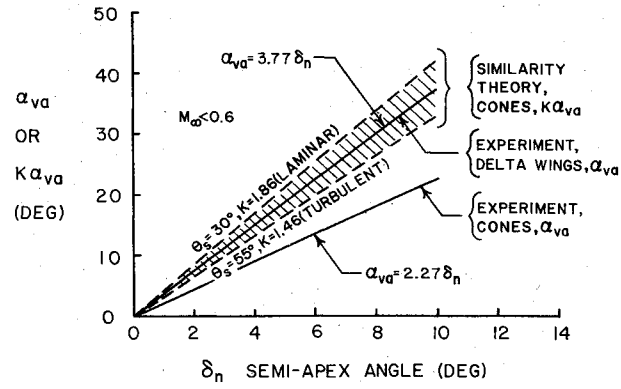


**Fig. 2 Experimental verification for circular cones.**

Eq. (2). The corresponding doublet conjugate complex velocity is $\hat{v}_D-i\hat{w}_D=i\hat{w}_\infty(h^2-a^2)/(\hat{X}+ih)^2$. Expanding this expression in powers of $(\hat{X}/ih)$ for $|\hat{X}/ih|\ll 1.0$ and retaining the leading term only yields the uniform vertical stream $\hat{w}_0=[1-(a^2/h^2)]\bar{w}_\infty$, where the subscript zero denotes this specialized result. The equivalent uniform stream $\bar{w}_\infty$ in the $\bar{X}$ plane is taken equal to $\hat{w}_0$, yielding the result

$$\tilde{k}=1-\tan^2(\tilde{\theta}_s/2) \tag{7}$$

where use has been made of Eq. (6) and $\tilde{\theta}_s$ is given by Eq. (5). The angles of attack in the $X^*$ and $X$ planes are related by

$$\alpha^*=K\alpha \qquad \text{where} \quad K\equiv 2k\tilde{k} \tag{8}$$

For a laterally symmetric body of arbitrary cross section in the $x, y, z$ space, the relation for $k$ will differ from Eq. (4) with the explicit form depending upon the body cross-sectional shape and the mapping function employed. The form of the relation for $\tilde{k}$, Eq. (7), will remain unchanged. The specific relation for $\tilde{\theta}_s$ to be used in Eq. (7), however, will depend on the aforementioned mapping function and will therefore differ from Eq. (5).

In summary, for a laterally symmetric separated vortex flow about a laterally symmetric body of arbitrary cross section and planform in the $x, y, z$ space, Eq. (8) (by means of the parameter $K$) relates the local angle of attack at a given body $x$ station to the local angle of attack for the flow about a zero-thickness wing with the same planform as the original body but with the separation points approximately transformed conformally to the wing leading edges. For the most general configurations $K$ will be a function of $x$, since $\theta_s$ is a function of $x$, and it will be necessary to place the "equivalent" zero-thickness wing in a nonuniform cross-flow stream to achieve similarity in the sense just described, or alternatively the wing could be longitudinally cambered to conform to the stream nonuniformity. Although similarity comparisons for geometries with variable $\theta_s$ represent a possibility, such comparisons are unwieldly and appropriate experimental data likely unavailable. Slender elliptic and circular cones are more promising candidates for comparison, since $\theta_s$ is constant for these configurations, the required similarity cross-flow stream for the equivalent wing is uniform, and appropriate experimental data are available.

For interpretation of vortex-asymmetry onset, Eq. (8) is applied at the vortex-asymmetry-onset condition and becomes

$$\alpha^*_{va}=K\alpha_{va} \tag{9}$$

where the asterisk denotes the equivalent zero-thickness wing, the subscript $va$ denotes vortex-asymmetry onset, and $K$ [defined in Eq. (8)] is constant for elliptic and circular cones. If comparison with experiment verifies Eq. (9), it may be

inferred, for the reasons set forth by Keener and Chapman,[1] that vortex-asymmetry onset is due principally to a hydrodynamic instability phenomenon rather than to the occurrence of laterally asymmetric viscous separation. The foregoing considerations assume that vortex bursting has not occurred forward of the trailing edge.

### Experimental Verification

Experimental representations for the onset angle of attack $\alpha_{va}$ for vortex asymmetry as a function of semiapex angle $\delta_n$ are shown in Fig. 2 for flat delta wings and circular cones. The experimental data points have been represented by faired straight lines for the sake of clarity. The data for the delta wings are taken from Refs. 3-6, whereas those for the circular cones are taken from Refs. 7-10. The straight-line slope for the cone data differs slightly from that used by Keener and Chapman[1] because of the use of a different onset criterion. Details regarding the interpretation of the experimental data may be obtained by contacting the author.

The consequence of application of the similarity parameter $K$ to experimental circular-cone vortex-asymmetry data for lateral separation angles ranging from laminar separation ($\theta_s = 30$ deg) to turbulent separation ($\theta_s = 55$ deg) is shown by the crosshatched region in Fig. 2. It is seen here that the application of the similarity parameter brings the cone data into general agreement with the delta wing data.

### Concluding Remarks

The foregoing analysis is not intended to be a definitive treatment of the subject of vortex-asymmetry onset, but rather to provide some insight into a complicated phenomenon by means of a simple analytic model. If one accepts the approximations involved, the analysis favors attributing vortex-asymmetry onset for delta wings and circular cones to a hydrodynamic instability phenomenon. This does not preclude the possibility of a viscous asymmetric separation cause and effect, but such a determination requires a more rigorous analysis than the one presented herein.

### References


[1] Keener, E. R. and Chapman, G. T., "Similarity in Vortex Asymmetries over Slender Bodies and Wings," *AIAA Journal*, Vol. 15, Sept. 1977, pp. 1370-1372.

[2] Ericsson, L. E. and Reding, J. P., "Steady and Unsteady Vortex-Induced Asymmetric Loads on Slender Vehicles," *Journal of Spacecraft and Rockets*, Vol. 18, March-April 1981, pp. 97-109.

[3] Shanks, R. E., "Low-Subsonic Measurements of Static and Dynamic Stability Derivatives of Six Flat-Plate Wings Having Leading-Edge Sweep Angles of 70° to 84°," NASA TND-1822, 1963.

[4] Bird, J. D., "Tuft-Grid Surveys at Low Speeds for Delta Wings," NASA TND-5045, Feb. 1969.

[5] Polhamus, E. C., "Predictions of Vortex-Lift Characteristics by a Leading-Edge Suction Analogy," *Journal of Aircraft*, Vol. 8, April 1971, pp. 193-199.

[6] Erickson, G. E., "Vortex Flow Correlation," Air Force Systems Command, Tech. Rept. AFWAL-TR-80-3143, Jan. 1981.

[7] Coe, P. L. Jr., Chambers, J. R., and Letko, W., "Asymmetric Lateral-Directional Characteristics of Pointed Bodies of Revolution at High Angles of Attack," NASA TND-7095, 1973.

[8] Orlik-Rückemann, K. J., LaBerge, J. G., and Iyengar, S., "Half- and Full-Model Experiments on Slender Cones at Angles of Attack," *Journal of Spacecraft and Rockets*, Vol. 10, Sept. 1973, pp. 575-580.

[9] Keener, E. R., Chapman, G. T., Cohen, L., and Taleghani, J., "Side Forces on Forebodies at High Angles of Attack and Mach Numbers from 0.1 to 0.7: Two Tangent Ogives, Paraboloid and Cone," NASA TM X-3438, 1976.

[10] Peake, D. J. and Owen, F. K., "Control of Forebody Three-Dimensional Flow Separation," Paper 17 in AGARD-CP-262, Sept. 1979.


AIAA 82-4097

# Axisymmetric Inviscid Swirling Flows Produced by Bellmouth and Centerbody


Yoshiaki Nakamura,* Toshio Hama† and Michiru Yasuhara‡

*Nagoya University, Nagoya, Japan*


### Introduction

MANY researchers, such as Harvey,[1] Sarpkaya,[2-4] and Faler and Leibovich,[5,6] have used similar apparatus to conduct experiments on vortex breakdown in a pipe. The equipment to generate the swirling flows consists of bellmouth and centerbody. Generally, the vortex breakdown might be affected by the upstream flow conditions in the pipe. Therefore, it is significant to examine the flows produced by the swirl flow generating equipment. In addition, these might be used as part of the upstream conditions for numerically calculating the swirling flows in the pipe.

According to several experiments, the axial velocity component profile around the upstream cross section of the pipe characteristically has a high velocity near the axis. The circumferential velocity component shows the solid rotation around the pipe axis and the irrotational swirl at the outer region when the Reynolds number is high. Faler and Leibovich[5] represented least square best fit of the experimental data to the profiles $W(r) = W_1 + W_2\exp(-\alpha r^2)$, $V(r) = Kr^{-1}[1-\exp(-\alpha r^2)]$, which correspond to the axial and circumferential velocity components, respectively. $W_1$, $W_2$, $\alpha$, and $K$ are arbitrary constants, and $r$ is the radial location.

The objective of the present Note is to partially explain these characteristics by actually calculating the flow between the bellmouth and centerbody. Although two kinds of effects, large deformation of geometry and viscosity, should be considered, for simplicity we consider only the effect of large deformation and show to what extent the flow can be simulated due to the large deformation. The results are compared with the experimental ones.

### Governing Equation

The equations are written in cylindrical coordinates $(r,\theta,z)$, where $u$, $v$, and $w$ are the velocity components in the $r$, $\theta$, and $z$ directions, respectively, as shown in Fig. 1. For axisymmetric inviscid swirling flows, the basic equation is written as follows[4]:

$$\frac{\partial^2\psi}{\partial r^2} - \frac{1}{r}\frac{\partial\psi}{\partial r} + \frac{\partial^2\psi}{\partial z^2} + K\frac{dK}{d\psi} - r^2\frac{dE}{d\psi} = 0 \qquad (1)$$

where $\psi$ represents the stream function, $K(\psi)$ the circulation function defined by $K = vr$, and $E(\psi)$ the total energy per mass. The variables are nondimensionalized by the following quantities: $r$, $z$, the pipe radius $R$; $u$, $v$, $w$, the pipe mean velocity $Wm$; $\psi$, $Wm^2R$; $E$, $Wm^2$; and $K$, $WmR$.

Boundary conditions were treated in the following manner.

Received May 29, 1981; revision received Sept. 8, 1981. 


*Research Associate, Dept. of Aeronautical Engineering, present address, NRC Research Associate, NASA Ames Research Center. Member AIAA.

†Graduate Student.

‡Professor, Department of Aeronautical Engineering.